Hindawi
Shock and Vibration
Volume 2020, Article ID 3918352, 12 pages
https://doi.org/10.1155/2020/3918352

Research Article

Numerical Analysis of Seismic Site Effects in Loess Region of Western China under Strong Earthquake Excitations

Tuo Chen,[1,2] Zhijian Wu,[3] Yanhu Mu,[2] Ping Wang,[4] and Qiyin Zhu[1]

[1]*State Key Laboratory for Geomechanics and Deep Underground Engineering, China University of Mining and Technology, Xuzhou 221116, China*
[2]*State Key Laboratory of Frozen Soil Engineering, Chinese Academy of Sciences, Lanzhou 730000, China*
[3]*College of Transportation Science and Engineering, Nanjing Tech University, 30 South Puzhu Road, Nanjing 210009, China*
[4]*Lanzhou Institute of Seismology, CEA, Lanzhou 730000, China*

Correspondence should be addressed to Zhijian Wu; zhijianlz@163.com

Received 28 October 2019; Accepted 8 August 2020; Published 25 August 2020

Academic Editor: Ivo Caliò

The Loess Plateau is one of the most tectonically and seismically active areas in the world. Observations from past strong earthquakes, particularly the Minxian–Zhangxian and Wenchuan earthquakes, have shown distinctive evidence of seismic site effects in the mountainous area of southeastern Gansu province. In this study, seismic damage in the loess areas of southeastern Gansu province induced by these earthquakes was investigated and briefly described. Different types of ground motion were selected, and the one-dimensional equivalent linear method was used for numerical analysis of the ground motion effects in the loess regions. Moreover, seismic response analysis of a typical loess tableland was conducted. The results showed that the seismic responses of a typical loess tableland under different seismic excitations have totally different dynamic characteristics. Moreover, the seismic damage in loess regions was more serious under far-field seismic excitation compared with near-field seismic excitation with the same peak acceleration. Through this study, the quantitative assessment of ground motion effects can be approximately estimated and the mechanism of site amplification effects on ground motion is further explained.

1. Introduction

Loess and loessic deposits cover an area of 631,000 km^2 of the mainland of China, which accounts for approximately 6.6% of the total area of the country. The Loess Plateau is located on the upper and middle stream of the Yellow River, covering an area of 440,000 km^2 in the northwestern part of China. Loess thickness generally exceeds 100 m over large areas of the Loess Plateau, with a maximum recorded thickness of 335 m in eastern Gansu province near the city of Lanzhou [1]. Observations from past earthquakes have shown distinctive evidence of seismic site effects in the mountainous area of the southeastern Gansu province. Wu et al. [2] discussed the phenomena of site effects on ground motion in the mountainous area of southeastern Gansu province during the Wenchuan Ms8.0 earthquake. Wang et al. [3] concluded that amplification of ground motion by loess deposits caused additional damage during the Minxian–Zhangxian Ms6.6 earthquake. During these two devastating earthquakes, the seismic site effects in the form of amplification or deamplification were quite obvious.

The study of seismic site effects has been an issue of growing interest in recent years, and many resources have been devoted to explain the causes and impacts of these effects. The microtremor H/V spectral ratio method has been widely used for site effect studies. Authors such as Zaslavsky et al. [4], Bonnefoy-Claudet et al. [5], Lozano et al. [6], and Choobbasti et al. [7] have confirmed that the H/V spectral ratio approach provides an acceptable means of evaluating site effects in a study area. Furthermore, extensive research on site effects has been conducted using different numerical calculation methods. Pavlenko [8] simulated the propagation of vertically incident seismic waves in horizontal soil layers and studied the effects of nonlinearity in the seismic

response of soils. Bazzurro et al. [9] studied the effect of soil layers with uncertain properties on the ground motion intensity at the soil surface. Assimaki et al. [10] illustrated the important role of soil stratigraphy and material heterogeneity on the topographic aggravation of surface ground motion. Gatmiri et al. [11] evaluated seismic site effects due to local topographical and geotechnical characteristics. Arslan et al. [12] confirmed the influence of the nonlinearity of the soil behavior and elucidated the effect of nonlinearity on site response. Hartzell et al. [13] studied the influence of topography on ground motion and evaluated topographic amplification using a variety of methods. Pandey et al. [14] discussed the influence of local site conditions on characteristics of strong ground motion records, and their further effects on hazard studies were investigated. Tran et al. [15] discussed the influence of random variations in soil characterization on the seismic site response. Glinsky et al. [16] discussed the topographical and geological site effects based on a discontinuous Galerkin finite element method.

Seismic site effects are an important aspect in seismic hazard analysis. Tsai [17] proposed a method for probabilistic seismic hazard analysis considering nonlinear site effects. Based on his methodology, which incorporates the amplification of local soil deposits into the framework of probabilistic seismic hazard analysis, Bazzurro et al. [18] developed effective probabilistic procedures for evaluating ground motion hazards. Shreyasvi et al. [19] conducted standard probabilistic seismic hazard analysis combined with local site effects.

However, there are not many related studies about seismic site effects in the loess regions of western China. Several researchers, such as Wang et al. [20], Chen et al. [21], and Zhang et al. [22] tried to assess the site effects in loess regions on the basis of data obtained during field investigations and by applying a numerical analysis method. Although some conclusions were drawn after qualitative analysis and calculation, the quantitative assessment of ground motion effects should be further investigated, especially under different earthquake excitations. In this study, seismic damage in loess areas of southeastern Gansu province induced by the Minxian–Zhangxian earthquake and the Wenchuan earthquake was investigated. Different types of ground motion were selected, and the one-dimensional equivalent linear method was used for numerical analysis of the ground motion effects in these loess regions. Moreover, seismic response analysis of a typical loess tableland was conducted to further elucidate the mechanism of site amplification effects on ground motion. The results of this research will be of relevance for researchers and civil engineers and provide some guidance for minimizing earthquakes and preventing disasters in the loess areas of China.

2. Seismic Damage Investigation

The Wenchuan Ms8.0 earthquake in 2008 and the Minxian–Zhangxian Ms6.6 earthquake in 2013 caused enormous buildings and houses to collapse. They also caused serious damage in the Loess Plateau. Based on seismic damage investigation after these devastating earthquakes, the site amplification effects on ground motion were very obvious. The influence of the isolated topography and steep slopes on the seismic damage and seismic intensity was significant, which mainly manifested as more severe seismic damage and higher seismic intensities. After the Wenchuan earthquake, a temporary strong motion array of three stations was installed near Wenxian County in Gansu province. The aftershocks of the Wenchuan earthquake recorded by the temporary strong motion array showed that the peak ground acceleration (PGA) at the top station was nearly 1.5 times larger than that at the bottom station [23].

The seismic damage characteristics and the seismic intensities can be different in the same area due to differences in topography, geomorphology, soil thickness, and altitude. For example, Liujiapo village (E104.974, W33.453) and Haoping village (E104.983, W34.442) are located in Wudu district, Longnan city, Gansu province. The altitude of Haoping village, at the top of the mountain, is 1811 m and the altitude of the Liujiapo village on the mountainside is 1485 m. The dominant frequency of the Haoping site was 1.85 Hz, and the dominant frequency of the Liujiapo site was 3.85 Hz. As shown in Figure 1, these two mountain villages on the Loess Plateau were devastated during the Wenchuan earthquake, but with different damage conditions. The adobe buildings in Haoping village almost completely collapsed, whereas the seismic damage to the adobe buildings in Liujiapo village was relatively slight. Different seismic damage characteristics were also observed in the same area during the Minxian–Zhangxian Ms6.6 earthquake. As shown in Figure 2, Majiagou village (E104.094, W34.560) and Xinglin (E104.075, W34.541) village in Minxian County are located in the meizoseismal area. The altitude of Majiagou village is 2512 m and the altitude of Xinglin village on the mountainside is 2303 m. The dominant frequency of the Majiagou site was 1.8 Hz, whereas the dominant frequency of the Xinglin site was 2.47 Hz. The seismic intensities and building destruction at these two sites were found to be significantly different.

3. Seismic Ground Motion Analysis

Site response analysis is crucial for defining the seismic hazard and distribution of damage during earthquakes. In this paper, the one-dimensional equivalent linear method is used to perform seismic ground motion analysis. This method is implemented based on elastic wave propagation theory, which assumes that the response of soil deposits is predominantly caused by the vertical propagation of shear wave from the bedrock. Each layer is assumed homogenous and isotropic and is characterized by its shear modulus, soil density, damping ratio, and thickness. The vertical propagation of shear wave through the system can be calculated by using the solution of the wave equation. The characteristic of this method is that the definite calculating parameters (such as the equivalent shear modulus and damping ratios) are used to describe the complex changes of the soil. Then, an iterative method is applied for dynamic response calculations; hence, the problem is changed from nonlinear to linear.

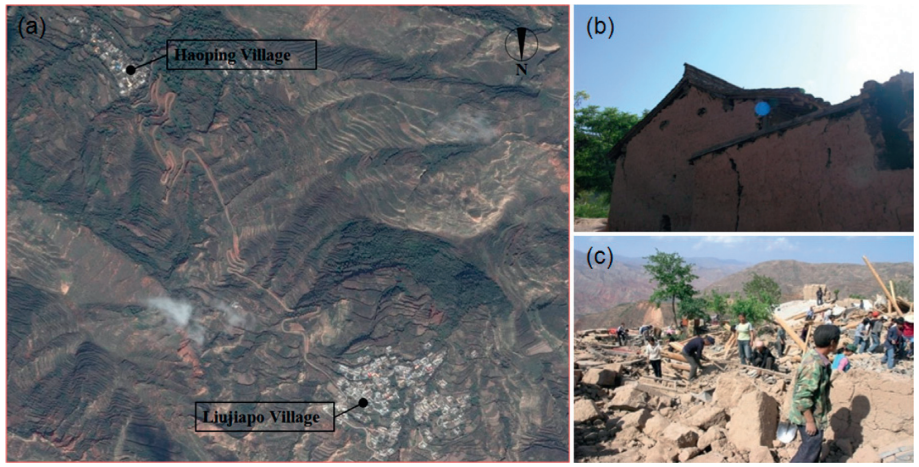

Figure 1: Differences in earthquake damage in two typical villages. (a) Topography of the two typical villages, (b) house damage in Liujiapo village, and (c) house damage in Haoping village.

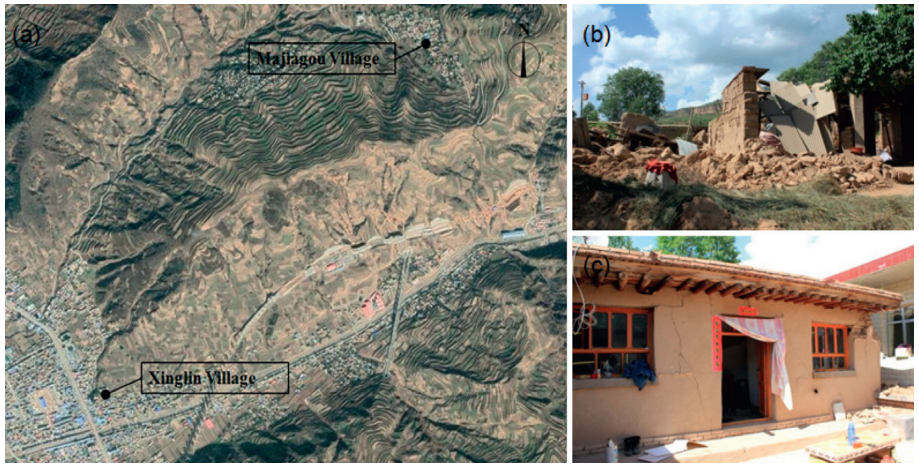

Figure 2: Differences in earthquake damage in two typical villages. (a) Topography of the two typical villages, (b) house damage in Majiagou village, and (c) house damage in Xinglin village.

3.1. Dynamic Parameters of Loess. The dynamic parameters of loess, including the shear modulus and damping ratios, change under different shear strain amplitudes. The shear modulus and damping ratios were determined by dynamic triaxial tests conducted by the Key Laboratory of Loess Earthquake Engineering, China Earthquake Administration. The dynamic parameters of typical loess are shown in Table 1. The dynamic shear modulus ratio (G/G_0) of typical loess decreases with increasing shear strain, whereas the damping ratio λ increases with increasing shear strain.

3.2. Input Seismic Motions. From a geological perspective, an earthquake's near-field is defined as the area within 20–50 km from the epicenter. Near-field earthquakes consist of a major portion of the fault energy in the form of pulses. These pulses tend to have a maximum Fourier spectrum in limited periods, whereas far-field earthquakes have a maximum Fourier spectrum in a broad range of periods [24]. In this study, considering the different earthquake characteristics, two groups of ground motion time histories were taken as the input seismic motions for the seismic site response analysis.

The horizontal earthquake accelerogram in the N–S direction, recorded at the Minxian seismostation during the 2013 Minxian–Zhangxian Ms6.6 earthquake, was selected as the near-field seismic motion (Minxian seismic motion). The epicenter of this earthquake was located at (W34.5°, E104.2°) and the seismostation was 18 km away from the epicenter. Figure 3 indicates the Minxian seismic motion and its spectrum characteristics. The maximum acceleration of the input motion was 219 cm s^{-2}, and the energy of the earthquake ground motion was concentrated in the range of 3–10 Hz.

The other horizontal earthquake accelerogram in the E–W direction, recorded at Tianshui seismostation during the 2008 Wenchuan Ms8.0 earthquake, was selected as the far-field seismic motion (Tianshui seismic motion). The epicenter of this earthquake was located at (W31.01°, E103.42°) and the seismostation was 415 km away from the

Table 1: The dynamic parameters of typical loess.

Index	Shear strain ($\times 10^{-4}$)							
	0.05	0.1	0.5	1	5	10	50	100
G/GO	0.965	0.914	0.885	0.750	0.634	0.288	0.110	0.055
λ	0.008	0.015	0.031	0.043	0.072	0.129	0.173	0.205

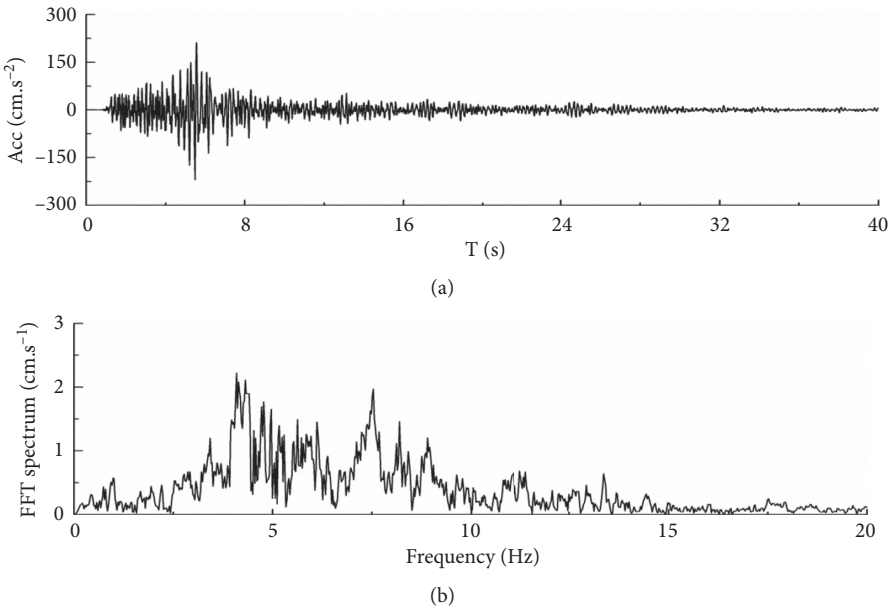

Figure 3: Accelerogram recorded at Minxian seismostation during the Minxian–Zhangxian earthquake.

epicenter. Figure 4 indicates the Tianshui seismic motion and its spectrum characteristics. The maximum acceleration of the input motion was 209 cm s^{-2}, and the energy of earthquake ground motion was concentrated in the range of 0.5–4 Hz.

3.3. Numerical Computation Scheme. A numerical scheme is presented to compute the seismic response of the loess site. Figure 5 presents the one-dimensional idealization calculation model. As shown in Figure 5, this calculation model contained two layers: the upper loess layer and the bottom bedrock layer. The thickness of the upper loess layer was set to be a variable quantity H, which ranged from 5 to 100 m; the thickness of the bottom bedrock layer was also invariant.

It was assumed that the loess soils at various depths have the same values of shear modulus and damping ratios, but different densities and shear wave velocities. The relevant parameters of the one-dimensional model are illustrated in Table 2. The shear wave velocities of the soil layers at different depths in Table 2 are determined according to the field shear wave velocity and laboratory tests. The field shear wave velocity tests were carried out in the mountainous areas of southeastern Gansu province where the loess is more than 100 m thick [25]. Then the dynamic calculation was performed with different loess thicknesses by applying the one-dimensional equivalent linear method.

3.4. Numerical Results Analysis. Figure 6 illustrates the ground motion acceleration time history at loess sites with different loess layer thicknesses under the above two seismic loads. The phase difference of the ground motion at the loess site considering the influence of the soil thickness is relatively small. The peak ground acceleration increases with increasing loess layer thickness, demonstrating the magnification effect of seismic motion in the loess region.

The distribution curves of the PGA amplification coefficients are presented in Figure 7. It was found that the dynamic magnification effects under different seismic waves had distinctive characteristics. The amplification coefficient gradually increased with increasing soil layer thickness under the Tianshui seismic excitation, with a maximum amplification coefficient of nearly 2.4. However, under the Minxian seismic excitation, the amplification coefficient had nonlinear characteristics. The coefficient rapidly increased, and significant magnification was observed at a thickness of 15 m. As the soil layer thickness further increased, the coefficients initially decreased then slowly increased. Compared with the coefficient under the Tianshui earthquake excitation, this value was greater when the thickness was less than 40 m. When the soil layer thickness was greater than 60 m, the coefficient was smaller. The maximum amplification coefficient was 2.2.

The normalized acceleration response spectra of the loess site under different seismic waves are illustrated in Figure 8.

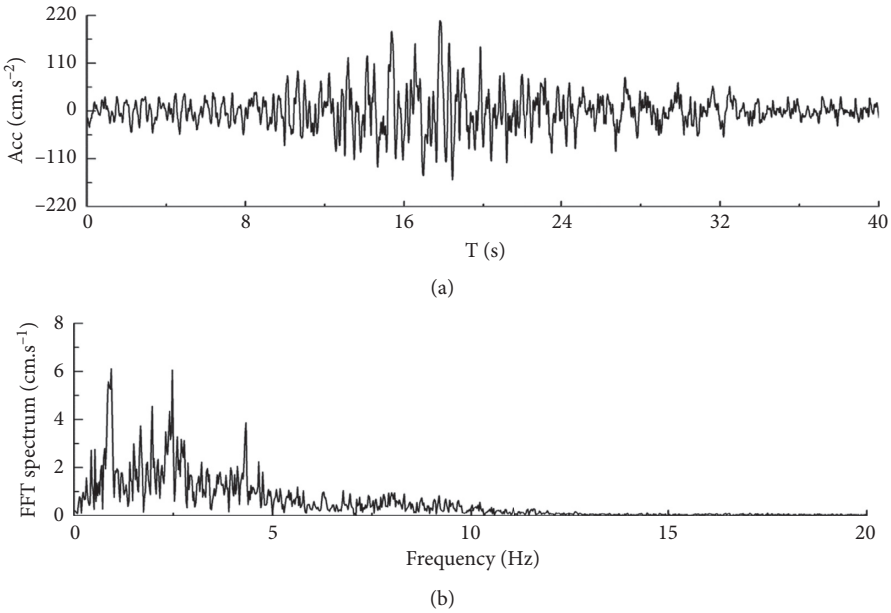

Figure 4: Horizontal acceleration history recorded at Tianshui seismostation during the Wenchuan earthquake.

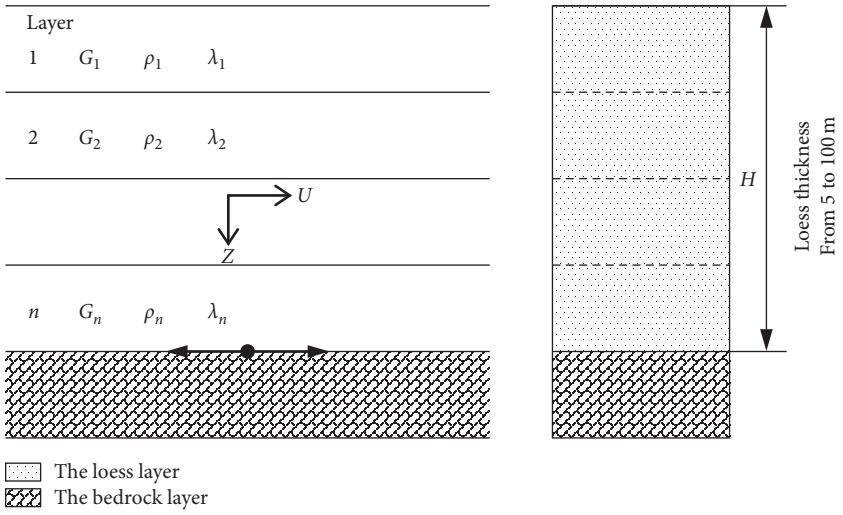

Figure 5: One-dimensional idealization calculation model.

It can be seen that structures with different natural vibration periods in the loess region had different dynamic responses under the earthquake excitation. The dynamic magnification factors in the loess region were mainly determined by the loess thickness, and they had different distribution characteristics under different seismic excitations. Under the Minxian earthquake excitation, the maximum dynamic magnification factors of the structures ranged from 3.9 to 4.9 when the depth of the loess layer was between 20 and 30 m. However, under the Tianshui earthquake excitation, the value of the dynamic magnification factor of the short-period structures (less than 1 Hz) was 4.3 when the depth of loess layer was 30 m. The value of the dynamic magnification factor of the long-period structures (greater than 1 Hz) was 4.8 when the soil layer thickness was 100 m.

4. Seismic Response of Loess Tableland

4.1. Numerical Model and Mechanical Parameters. To discuss the topographical effects on the dynamic behavior under earthquake excitation in the loess regions, dynamic analysis of the typical loess tableland was carried out by applying the nonlinear dynamic finite element analysis method.

According to the field investigation, the most common tableland in eastern Gansu province has a typical broken-line sloping surface, and the thickness of the loess layer is about 100 m. Figure 9 illustrates the numerical model of a typical loess tableland. The finite element model comprised two layers: the upper loess layer and the bottom bedrock layer. The loess was divided into five layers (ranging from ① to ⑤) and the thickness of each layer ranged from 15 to

Table 2: Soil parameters of one-dimensional model.

Lithology	Thickness (m)	Depth (m)	Density (kN·m^{-3})	V_s (m·s^{-1})
Loess	5	5	15.5	180
	5	10	16.0	200
	5	15	16.3	230
	5	20	16.5	280
	5	25	16.8	300
	5	30	17.0	340
	5	35	17.1	370
	5	40	17.3	420
	5	45	17.4	450
	5	50	17.6	480
	5	55	17.8	490
	5	60	18.0	510
	5	65	18.2	520
	5	70	18.4	530
	5	75	18.5	530
	5	80	18.7	540
	5	85	18.9	550
	5	90	19.1	560
	5	95	19.2	560
	5	100	19.5	570
Bedrock			22.0	800

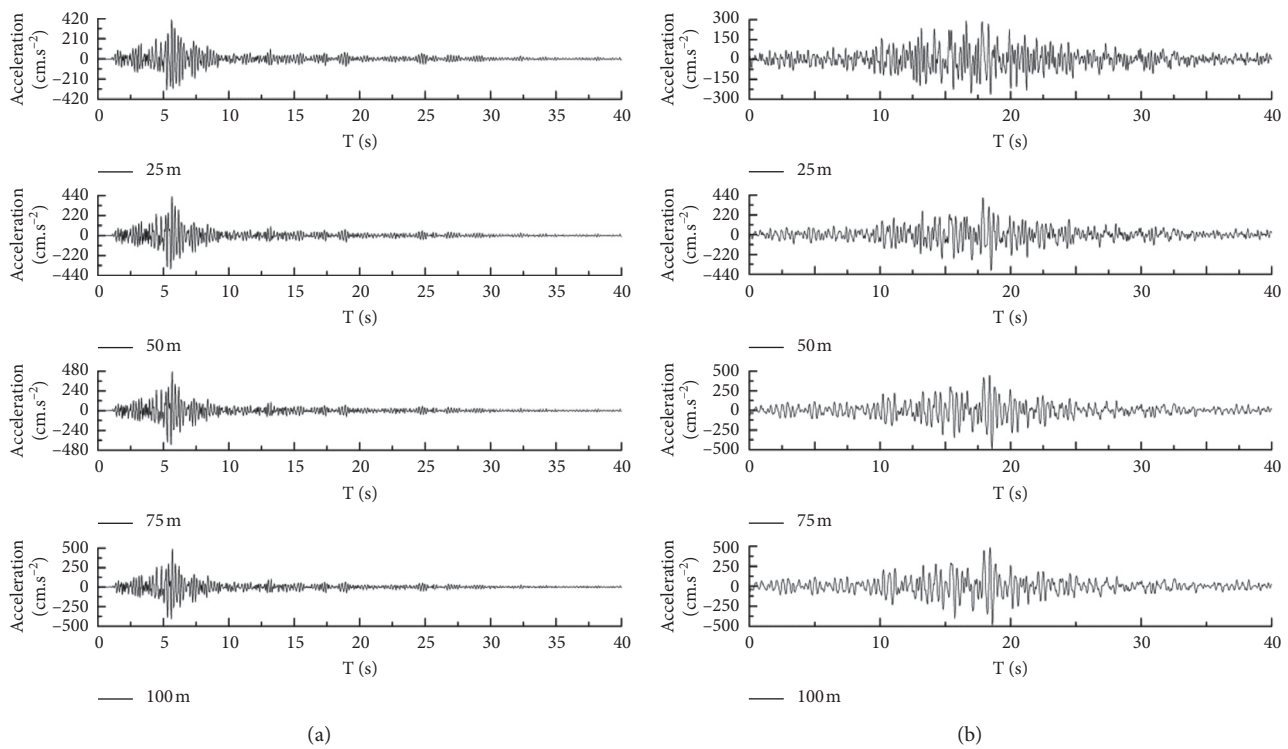

Figure 6: Ground motion acceleration time history of the sites with different overburden thicknesses. (a) Minxian seismic motion. (b) Tianshui seismic motion.

25 m. The different densities and mechanical parameters, corresponding to a one-dimensional model, were also given. The upper part of the tableland had an angle of 45° and the lower part of the tableland was at 60°. The heights of the upper part and lower part were 35 and 60 m, respectively.

In this simulation, the numerical calculation was deduced based on the plane strain assumption. In order to reduce the effect of boundary conditions on energy reflection and transmission properties, the coupling method of finite and infinite elements is presented. The infinite

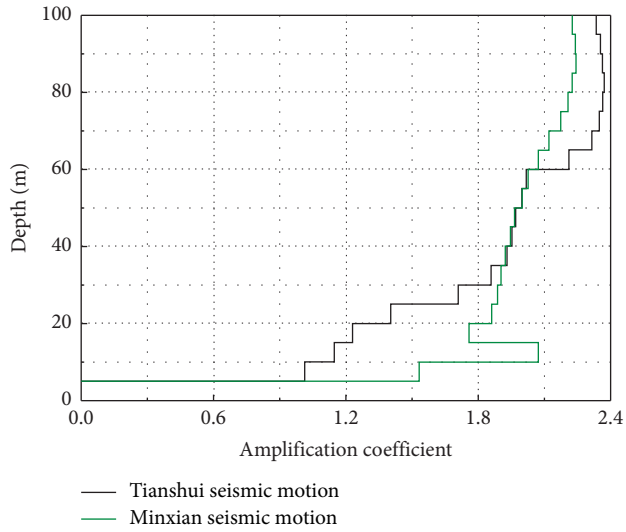

Figure 7: The distribution of the PGA amplification coefficients.

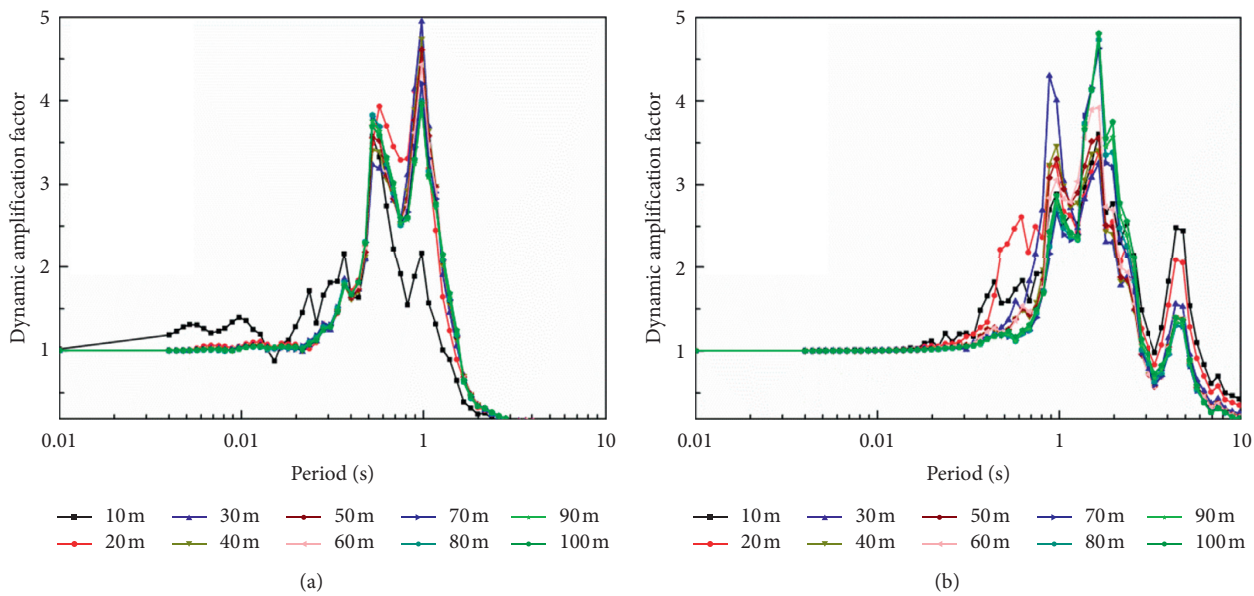

Figure 8: Acceleration spectra under the earthquake excitations. (a) Minxian seismic motion. (b) Tianshui seismic motion.

elements were used to simulate the lateral boundary conditions, and the artificial boundary condition was used for the bottom boundary. The horizontal direction at the bottom was released, and the different seismic waves (Figures 3 and 4) were used as the input seismic motions for the numerical calculation. Three observation points were arranged in the model: on the top (T), in the middle (M), and at the bottom (B).

Before carrying out the dynamic calculation, the dynamic response characteristics of free field soil were evaluated using an equivalent linear approach. Then, the soil values of the dynamic shear modulus and damping ratio were finally determined during maximum shear strain. In dynamic finite element analysis, the soil is regarded as an elastic-plastic material and the shear modulus (G_{max}) is related to the shear wave velocity (V_s) and the mass density (ρ) of a material through the relationship

$$G_{max} = \rho V_s^2. \quad (1)$$

In (1), V_s and ρ were decided corresponding to soil parameters of the one-dimensional model in Table 2. Moreover, elastic perfectly plastic constitutive model describing the soil behavior using the Mohr coulomb yield criterion is adopted [26]. The soil mechanical parameters for finite element numerical calculation, which are shown in Table 3, were obtained by triaxial tests [27].

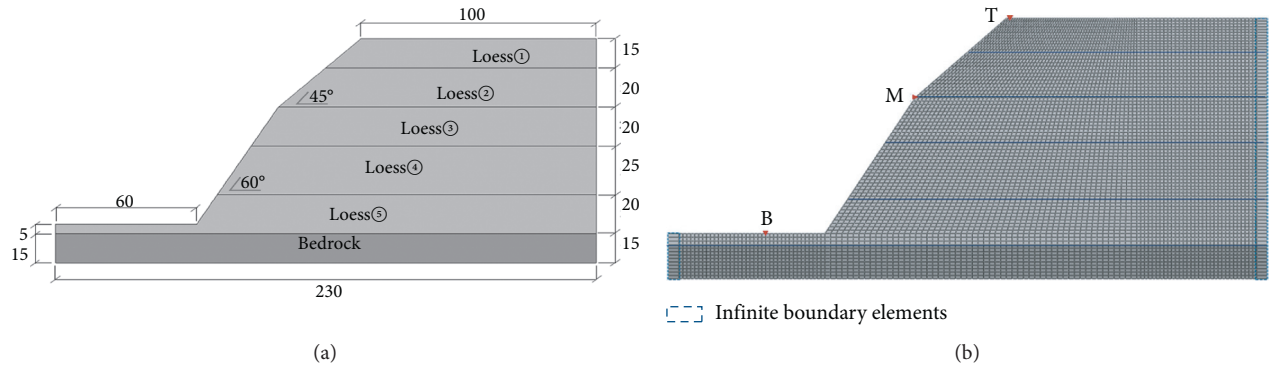

Figure 9: Models of finite element analysis. (a) Profile of the loess slope (unit: m) and (b) finite element model.

Table 3: Soil mechanics parameters of the finite element model.

Lithology	Thickness (m)	Density (kN·m^{-3})	Shear modulus (Pa)	Poisson's ratio	Cohesion (kPa)	Frictional angle
Loess ①	15	16.3	8.62E + 07	0.3	32	18°
Loess ②	20	17.0	1.97E + 08	0.3	35	18°
Loess ③	20	17.6	4.06E + 08	0.3	38	19°
Loess ④	25	18.5	5.20E + 08	0.3	42	20°
Loess ⑤	20	19.2	6.02E + 08	0.3	46	21°
Bedrock	15	22.0	1.41E + 09	0.2	120	34°

4.2. Acceleration Response of Loess Tableland. The seismic acceleration distribution characteristics of the loess tableland are discussed through the numerical analysis. Figure 10 illustrates the horizontal acceleration contour map under different seismic excitations. It can be intuitively observed that the maximum acceleration response occurs at different positions of the tableland. The maximum acceleration response occurs at the bottom of the tableland under the Minxian seismic excitation, whereas the maximum response occurs at the top of the tableland under the Tianshui seismic loading. Moreover, the peak ground acceleration increases with increasing slope height.

Figure 11 illustrates the amplification coefficient distribution as a function of the distance at the bottom of the tableland. In this figure, O is a point located at the slope toe and the direction of x-axis is away from the slope toe. There is an amplification area at the bottom of the tableland with an approximate width of 40 m. The amplification coefficient initially increased and then decreased with increasing distance. Moreover, there was slight amplification under the Tianshui seismic excitation, and the greatest coefficient was 2.1. This amplification was significant under the Minxian seismic excitation, and the greatest coefficient was 3.0.

Figure 12 illustrates the amplification coefficient distribution as a function of distance at the top of the tableland. In this figure, point O is a leading-edge location of the tableland and the direction of the x-axis is away from the leading edge. The amplification coefficient decreased with increasing distance, and significant amplification occurred within 15 m from the leading-edge location. Furthermore, this amplification was much greater than that under the Tianshui seismic excitation. The coefficient reached 4.9, whereas it was 1.9 under the Minxian seismic excitation.

4.3. Spectrum Characteristics. According to the relevant studies, the spectrum characteristics of the strong motion at different positions of the loess tableland varied. The acceleration time histories of the different observation points (Figure 9) were extracted, and the spectrum characteristics are also discussed in this paper. Figure 13 illustrates the acceleration time histories and the spectrum characteristics of the different points under the Minxian seismic excitation. The peak accelerations of different observations were 6.57 m s^{-2} (point B), 3.14 m s^{-2} (point M), and 3.86 m s^{-2} (point T). The dominant frequencies of the different observations were 4.8 Hz (point B), 4.3 Hz (point M), and 4.0 Hz (point T). Figure 14 illustrates the acceleration time histories and the spectrum characteristics of the different points under the Tianshui seismic excitation. The peak accelerations of the different observations were 4.3 m s^{-2} (point B), 5.1 m s^{-2} (point M), and 10.0 m s^{-2} (point T). The dominant frequencies of the different observations were 4.3 Hz (point B), 2.5 Hz (point M), and 1.7 Hz (point T).

In summary, there was a delay in the peak acceleration time with the seismic wave propagation along the slope of the loess tableland. The ground motion at the top of the slope had the amplified low-frequency component, and the high-frequency components were filtered out. Moreover, the dominant frequency of the ground motion was lower when the observation point was located in the upper part of the loess tableland. This variation was more obvious under Tianshui seismic excitation.

4.4. Displacement Response. Figure 15 illustrates the relative horizontal displacement response of the observation points at different positions of the loess tableland under different

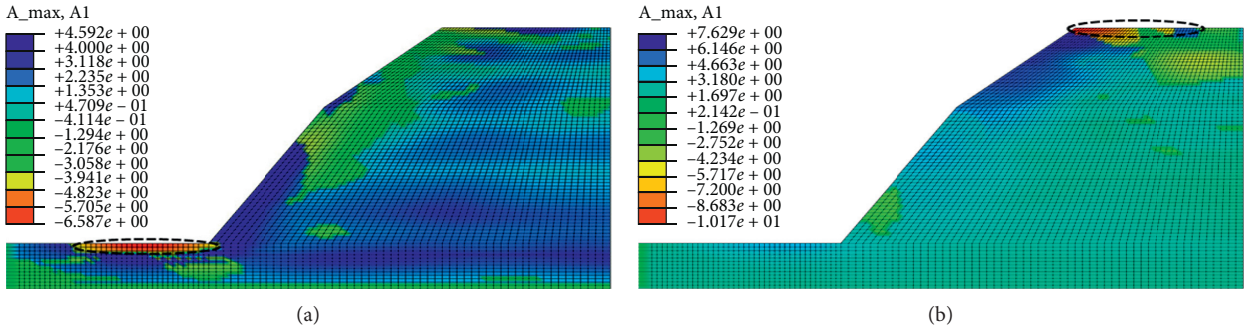

Figure 10: Horizontal acceleration contour map under different seismic excitations. (a) under Minxian seismic excitation. (b) under Tianshui seismic excitation.

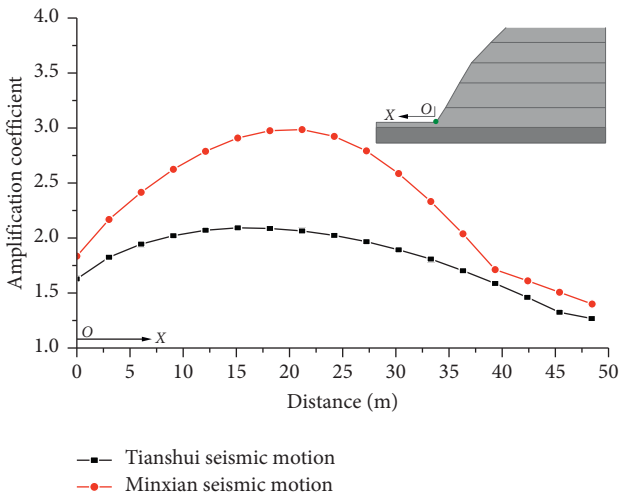

Figure 11: Distribution of the amplification coefficient with the distance.

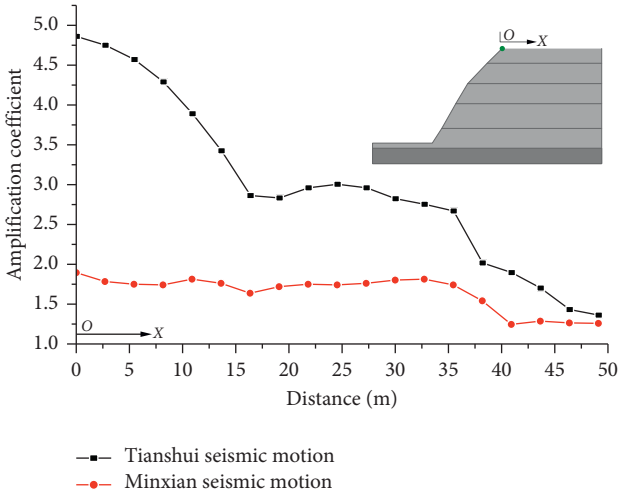

Figure 12: Distribution of the amplification coefficient with distance on the top of the loess tableland.

seismic excitations. The maximum displacements of the different observation points under the Minxian seismic excitation were 0.008 m (point B), 0.02 m (point M), and 0.04 m (point T). These displacements under the Tianshui seismic excitation were 0.005 m (point B), 0.08 m (point M), and 0.18 m (point T).

Given the analysis above, it can be concluded that the horizontal displacement increases with increasing height of the loess tableland. The horizontal displacement response of the loess tableland under far-field seismic excitation is significantly greater than that under near-field seismic excitation. The horizontal displacement of the upper part of the tableland under the Tianshui seismic excitation is about five times greater than that under the Minxian seismic excitation. The numerical results illustrate that the seismic damage in loess regions is more serious under far-field seismic excitation compared with that under near-field seismic excitation with the same peak acceleration.

5. Discussion

From the above numerical analysis results, it can be clearly seen that the seismic motion has a decisive influence on the site seismic response, and the seismic response of a typical loess tableland under different seismic excitations has totally different dynamic characteristics. Consequently, seismic damage characteristics in loess areas under different seismic excitations are also different. The reason can be summarized as follows.

First, the seismic amplification and soil-filtering effects play a crucial role in determining the seismic site effect. Far-field seismic waves have abundant low-frequency components, whereas near-field seismic waves are characterized by abundant high-frequency components. The soil-filtering effect is correlated with the soil thickness of the sites, and the amplification effect for different frequency components is not the same. Hence, the seismic ground motion under different seismic excitations could have different amplitudes and different response spectra.

Furthermore, at different positions of the loess tableland, the strong ground motion has different frequency components under the action of earthquakes. The dominant frequency of the strong motion at the bottom of the tableland is greater than that on the top of the tableland. Moreover, the dominant frequency of the loess site is related to the topography, geomorphology, soil thickness, and altitude. The site-predominant frequencies of different observation points in the epicenter of the Minxian–Zhangxian Ms6.6 earthquake, determined from microtremor measurements, are

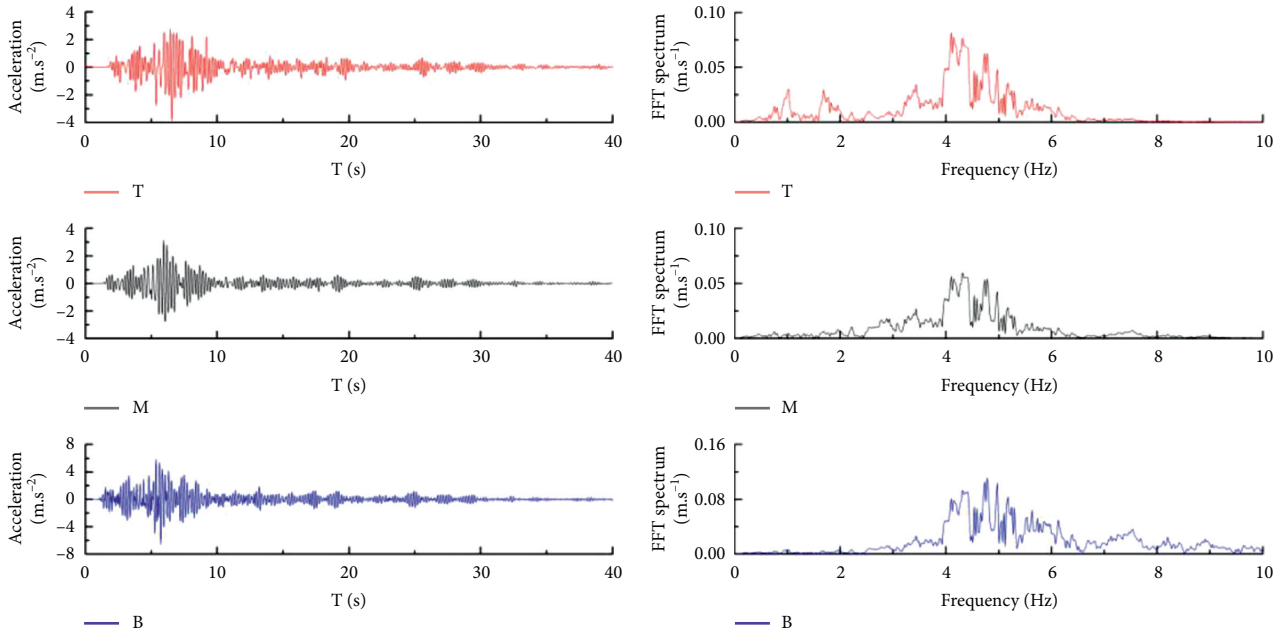

Figure 13: Ground motion characteristics under Minxian seismic excitation: (a) acceleration time histories and (b) spectrum characteristics.

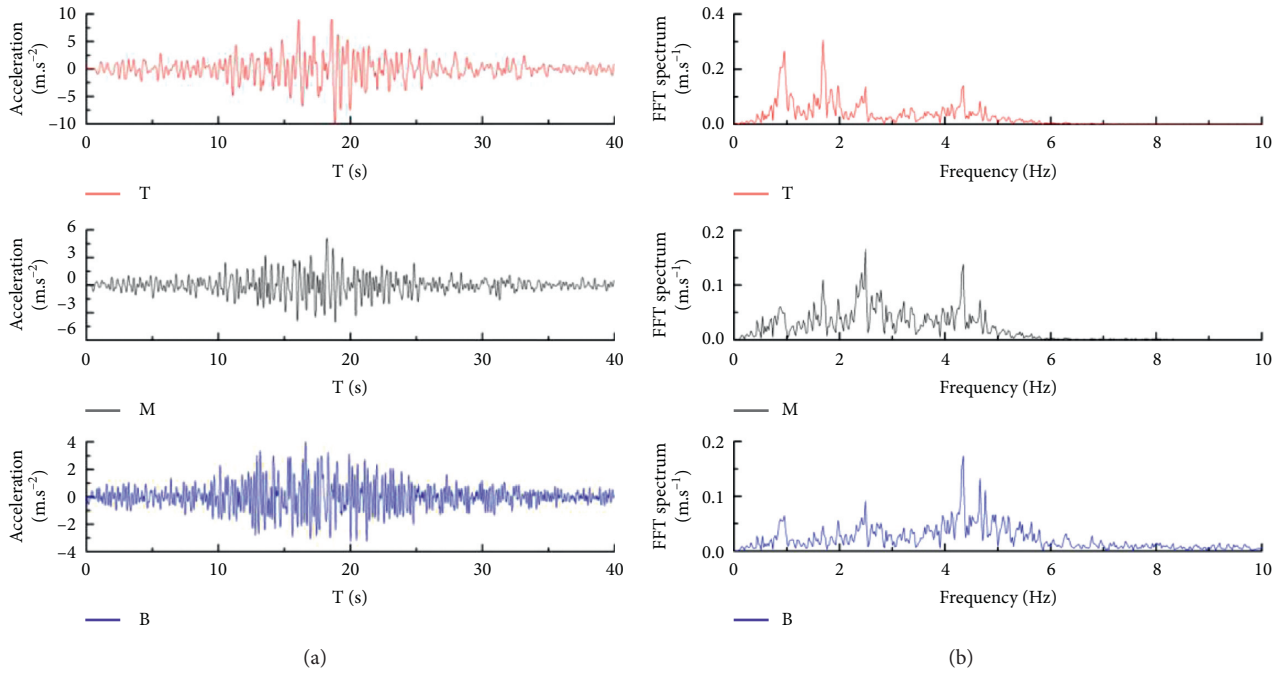

Figure 14: Ground motion characteristics under Tianshui seismic excitation: (a) acceleration time histories and (b) spectrum characteristics.

illustrated in Table 4. It can be intuitively observed that sites at lower altitudes have higher dominant frequencies. In addition to the theory of the reflection and refraction of seismic waves during the wave propagation, resonance theory may help explain the characteristics of the seismic response of loess tableland. The seismic response is strongest when the dominant frequency of the site is close to the dominant frequency of the strong motion.

Moreover, when the frequencies of far-field seismic motion are relatively low, then the structures in the loess

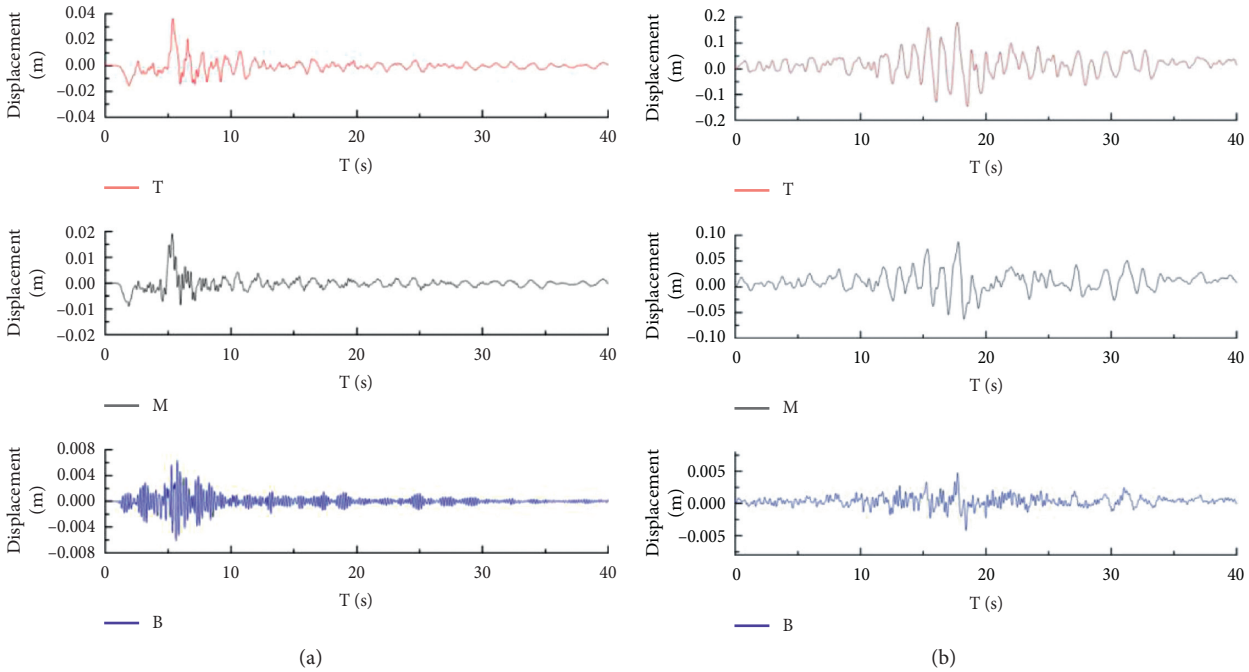

Figure 15: Displacement-time history curve under different seismic excitations: (a) under Minxian seismic excitation and (b) under Tianshui seismic excitation.

Table 4: The site-predominant frequencies of different observation points.

Observation point	Longitude and latitude	Altitude (m)	Dominant frequency (Hz)
Point 1	N 34°30′45″; E 104°10′8″	2775	1.6
Point 2	N 34°30′45″; E 104°9′41″	2626	1.5
Point 3	N 34°30′33″; E 104°9′30″	2645	1.3
Point 4	N 34°29′54″; E 104°8′00″	2375	5.6

area are prone to damage under this type of seismic motion because of the quasiresonance response. The dynamic magnification factors of the structures in loess regions are related to the loess thickness. The displacement response under the far-field seismic excitation is significantly greater than under the near-field seismic excitation. For these reasons, there are different seismic damage characteristics in the same area under different types of seismic motion.

6. Conclusions

Based on the seismic damage investigation, different types of ground motions were selected considering the different earthquake characteristics. Then, a seismic site response analysis was conducted; the seismic response of the loess tableland was also investigated. The numerical results indicated that the mechanism of seismic response is very complex and that seismic damage can vary in the same area. The main conclusions drawn from the computational analysis results are as follows:

(1) The seismic motion itself had a dominant influence on the site seismic response. The distribution of seismic damage in the same area was significantly different under different seismic excitations.

(2) The site amplification effect appears to have obvious nonlinear features under near-field earthquakes, whereas it shows an approximately linear trend under far-field earthquakes.

(3) Under near-field seismic excitation, the strongest seismic response occurs at the bottom of the tableland, whereas the strongest seismic response occurs at the top of the tableland under far-field seismic excitation.

(4) The seismic response is strongest when the dominant frequency of the site is close to the dominant frequency of the strong motion. The dominant frequency of the loess site should be assessed considering the influence of the topography, geomorphology, soil thickness, and altitude.

Data Availability

All data generated or analyzed during this study are included within this article.

Conflicts of Interest

The authors declare that there are no conflicts of interest regarding the work submitted.

Acknowledgments

This study was financially supported by the National Natural Science Foundation of China (nos. 41701058 and 41472297), the Open Fund of State Key Laboratory of Frozen Soil Engineering (Grant no. SKLFSE201606), and the China Postdoctoral Science Foundation (Grant no. 2015M570490).

References

[1] E. Derbyshire and T. W. Mellors, "Geological and geotechnical characteristics of some loess and loessic soils from China and Britain: a comparison," *Engineering Geology*, vol. 25, no. 2–4, pp. 135–175, 1988.

[2] Z. J. Wu, L. M. Wang, P. Wang, T. Chen, H. Shi, and X.-P. Yang, "Influence of site conditions on ground motion at far field loess sites during strong earthquake," *Journal of Central South University*, vol. 20, no. 8, pp. 2333–2341, 2013.

[3] L. M. Wang and Z. J. Wu, "Earthquake damage characteristics of the MinXian-ZhangXian Ms6.6 earthquake and its lessons," *China Earthquake Engineering Journal*, vol. 35, no. 3, pp. 401–412, 2013.

[4] Y. Zaslavsky, A. Shapira, and J. Leonov, "Empirical evaluation of site effects by means of H/V spectral ratios at the locations of strong motion accelerometers in Israel," *Journal of Earthquake Engineering*, vol. 7, no. 4, pp. 655–677, 2003.

[5] S. Bonnefoy-Claudet, C. Cornou, P.-Y. Bard et al., "H/V ratio: a tool for site effects evaluation. results from 1-D noise simulations," *Geophysical Journal International*, vol. 167, no. 2, pp. 827–837, 2006.

[6] L. Cotton, S. K. Herraiz, and S. K. Singh, "Site effect study in central Mexico using H/V and SSR techniques: independence of seismic site effects on source characteristics," *Soil Dynamics and Earthquake Engineering*, vol. 29, no. 3, pp. 504–516, 2009.

[7] A. J. Choobbasti, S. Rezaei, and F. Farrokhzad, "Evaluation of site response characteristics using microtremors," *Gradevinar*, vol. 65, no. 8, pp. 731–741, 2013.

[8] O. V. Pavlenko, "Nonlinear seismic effects in soils: numerical simulation and study," *Bulletin of the Seismological Society of America*, vol. 91, no. 2, pp. 381–396, 2001.

[9] P. Bazzurro and C. A. Cornell, "Ground-motion amplification in nonlinear soil sites with uncertain properties," *Bulletin of the Seismological Society of America*, vol. 94, no. 6, pp. 2090–2109, 2004.

[10] D. Assimaki, G. Gazetas, and E. Kausel, "Effects of local soil conditions on the topographic aggravation of seismic motion: parametric investigation and recorded field evidence from the 1999 Athens earthquake," *Bulletin of the Seismological Society of America*, vol. 95, no. 3, pp. 1059–1089, 2005.

[11] B. Gatmiri, C. Arson, and K. V. Nguyen, "Seismic site effects by an optimized 2D BE/FE method I. theory, numerical optimization and application to topographical irregularities," *Soil Dynamics and Earthquake Engineering*, vol. 28, no. 8, pp. 632–645, 2008.

[12] H. Arslan and B. Siyahi, "Effect of nonlinearity on site response and ground motion due to earthquake excitation," *Bulletin of Engineering Geology and the Environment*, vol. 69, no. 2, pp. 287–293, 2010.

[13] S. Hartzell, M. Meremonte, L. Ramirez-Guzman, and D. McNamara, "Ground motion in the presence of complex topography: earthquake and ambient noise sources," *Bulletin of the Seismological Society of America*, vol. 104, no. 1, pp. 451–466, 2014.

[14] B. Pandey, R. S. Jakka, and A. Kumar, "Influence of local site conditions on strong ground motion characteristics at Tarai region of Uttarakhand, India," *Natural Hazards*, vol. 81, no. 2, pp. 1073–1089, 2016.

[15] T.-T. Tran, S. R. Han, and D. Kim, "Effect of probabilistic variation in soil properties and profile of site response," *Soils and Foundations*, vol. 58, no. 6, pp. 1339–1349, 2018.

[16] N. Glinsky, E. Bertrand, and J. Régnier, "Numerical simulation of topographical and geological site effects. Applications to canonical topographies and Rognes hill, South East France," *Soil Dynamics and Earthquake Engineering*, vol. 116, pp. 620–636, 2019.

[17] C.-C. P. Tsai, "Probabilistic seismic hazard analysis considering nonlinear site effect," *Bulletin of the Seismological Society of America*, vol. 90, no. 1, pp. 66–72, 2000.

[18] P. Bazzurro and C. A. Cornell, "Nonlinear soil-site effects in probabilistic seismic-hazard analysis," *Bulletin of the Seismological Society of America*, vol. 94, no. 6, pp. 2110–2123, 2004.

[19] C. Shreyasvi, K. Venkataramana, and S. Chopra, "Local site effect incorporation in probabilistic seismic hazard analysis-a case study from Southern Peninsular India, an intraplate region," *Soil Dynamics and Earthquake Engineering*, vol. 123, pp. 381–398, 2019.

[20] S.-Y. Wang, Y.-X. Yu, and H.-S. Lü, "Study of characteristics of long-period ground motion response spectra by using broad-band records of the Chinese digital seismograph network," *Acta Seismologica Sinica*, vol. 11, no. 5, pp. 557–564, 1998.

[21] T. Chen, W. Ma, and J. Wang, "Numerical analysis of ground motion effects in the loess regions of Western China," *Shock and Vibration*, vol. 2017, Article ID 1484015, 9 pages, 2017.

[22] Z. Zhang, T. Wang, S. Wu, H. Tang, and C. Liang, "Seismic performance of loess-mudstone slope in Tianshui-centrifuge model tests and numerical analysis," *Engineering Geology*, vol. 222, pp. 225–235, 2017.

[23] L. M. LiangTang and Z. J. Wu, "Influence of site condition on seismic amplification effects during the Wenchuan earthquake," *Journal of Civil, Architectural & Environmental Engineering*, vol. 32, no. Supp.2, pp. 175–178, 2010.

[24] W. D. Iwan, "Important near-field ground motion data from the landers earthquake," in *Proceedings of the, 10th European Conference on Earthquake Engineering*, pp. 229–234, Vienna, Austria, August 1994.

[25] L.-M. Wang, Z.-J. Wu, and K. Xia, "Effects of site conditions on earthquake ground motion and their applications in seismic design in loess region," *Journal of Mountain Science*, vol. 14, no. 6, pp. 1185–1193, 2017.

[26] A. L. Che, T. Iwatate, and X. R. Ge, "Dynamic behaviors of subway structure subjected to strong earthquake motions using shaking table tests and dynamic analyses," *Rock and Soil Mechanics*, vol. 27, no. 8, pp. 1293–1298, 2006.

[27] Z. J. Wang, Y. S. Luo, R. R. Wang, L. G. Yang, and D. Y. Tan, "Experimental study on dynamic shear modulus and damping ratio of undisturbed loess in different regions," *Chinese Journal of Geotechnical Engineering*, vol. 32, no. 9, pp. 1464–1469, 2010.